A Three-Dimensional FRET Analysis to Construct an Atomic Model of the Actin–Tropomyosin–Troponin Core Domain Complex on a Muscle Thin Filament

A Three-Dimensional FRET Analysis to Construct an Atomic Model of the Actin–Tropomyosin–Troponin Core Domain Complex on a Muscle Thin Filament

Masao Miki [1]*, Satoshi Makimura [1], Yasuyuki Sugahara [1], Ryuta Yamada [1], Masashi Bunya [1], Takahiro Saitoh [1] and Hidetaka Tobita [2]

[1]*Division of Applied Chemistry and Biotechnology, Graduate School of Engineering Science, University of Fukui, Fukui 910-8507, Japan*
[2]*Division of Materials Science and Engineering, Graduate School of Engineering Science, University of Fukui, Fukui 910-8507, Japan*

It is essential to know the detailed structure of the thin filament to understand the regulation mechanism of striated muscle contraction. Fluorescence resonance energy transfer (FRET) was used to construct an atomic model of the actin–tropomyosin (Tm)–troponin (Tn) core domain complex. We generated single-cysteine mutants in the 167–195 region of Tm and in TnC, TnI, and the β-TnT 25-kDa fragment, and each was attached with an energy donor probe. An energy acceptor probe was located at actin Gln41, actin Cys374, or the actin nucleotide-binding site. From these donor–acceptor pairs, FRET efficiencies were determined with and without Ca^{2+}. Using the atomic coordinates for F-actin, Tm, and the Tn core domain, we searched all possible arrangements for Tm or the Tn core domain on F-actin to calculate the FRET efficiency for each donor–acceptor pair in each arrangement. By minimizing the squared sum of deviations for the calculated FRET efficiencies from the observed FRET efficiencies, we determined the location of Tm segment 167–195 and the Tn core domain on F-actin with and without Ca^{2+}. The bulk of the Tn core domain is located near actin subdomains 3 and 4. The central helix of TnC is nearly perpendicular to the F-actin axis, directing the N-terminal domain of TnC toward the actin outer domain. The C-terminal region in the I–T arm forms a four-helix-bundle structure with the Tm 175–185 region. After Ca^{2+} release, the Tn core domain moves toward the actin outer domain and closer to the center of the F-actin axis.

*Corresponding author. E-mail address:
mmiki@u-fukui.ac.jp.

Introduction

Striated muscle contraction is regulated by tropomyosin (Tm) and troponin (Tn) on the actin filament in response to a Ca^{2+} concentration change.[1] Rabbit skeletal muscle α-Tm, a 284-residue dimeric coiled-coil protein, contains seven quasi-equivalent regions and spans seven actin monomers along the two-start long-pitch F-actin

helix.[2] Tn consists of three subunits: TnT, TnI, and TnC. Ca^{2+} binding to TnC induces a conformational change in Tn, which is propagated along the actin filament by Tm. The mechanism for this regulatory process is not well defined. It is essential to know the detailed structure of the thin filament to understand the regulation mechanism. Although crystal structures of actin,[3] Tm,[4] and the Tn core domain[5,6] have been solved, it is uncertain how these components assemble to form the thin filament and how they change the spatial relationship during muscle activation. Because the thin filament is composed of hundreds of actin, Tm, and Tn molecules, it is difficult to crystallize such supramolecular assemblies. The atomic structure of G-actin was positioned in the actin filament helix by modeling with fiber X-ray diffraction patterns from aligned gels of actin filaments.[7,8] A more refined structure of F-actin has been reported by modeling with fiber X-ray diffraction patterns using magnetically aligned actin filaments[9] and electron cryo-microscopy.[10] However, it is unclear how the Tm–Tn complex interacts with the seven actin monomers in the thin filament and what conformational changes occur in the thin filament during activation upon Ca^{2+} binding to Tn. To date, structural models of the thin filament are primarily three-dimensional image reconstructions of electron microscopy (3D-EM) and X-ray diffraction measurements.[11–15] These models differ from each other on the location and orientation of Tn on an F-actin filament. Although the atomic structure of the Tn core domain has been determined, it is only part of the larger Tn molecule ($\sim 60\%$ of the mass). Therefore, it is difficult to precisely evaluate the Tn contribution to the 3D-EM and X-ray diffraction analyses.

Fluorescence resonance energy transfer (FRET) spectroscopy, which is an optical ruler for measuring the distance over a 10- to 70-Å range, has been extensively used to study the spatial relationships between residues in muscle proteins.[16,17] We systematically measured numerous intermolecular FRET efficiencies between probes attached to the Tn subunits and Tm on a reconstituted thin filament. These transfer efficiencies were compiled and analyzed for three-dimensional information. We constructed an atomic model of the Tn core domain and Tm complex by performing a global search for the rigid-body movements of the crystal structure to determine the position and orientation that minimize the deviation between the calculated and the observed FRET efficiencies.[18] By extending this method, we constructed an atomic model of the actin–Tm complex on a reconstituted thin filament with and without Ca^{2+}.[19] The atomic coordinates of Lorenz *et al.*'s F-actin model (the Lorenz model)[8] and the pig skeletal Tm crystal structure (Protein Data Bank code: 1C1G)[4] were used. The model shows which actin and Tm residues are involved in the interaction that includes electrostatic, hydrogen-bonding, and hydrophobic forces. The model did not show the Ca^{2+}-induced Tm azimuthal movement on F-actin, but it showed the substantial Ca^{2+}-induced changes at the actin–Tm contact surface, which are important for muscle regulation. In the study herein, we measured more than a hundred different transfer efficiencies between probes attached to the Tn core domain and probes attached to actin in a reconstituted thin filament with and without Ca^{2+}. The atomic coordinates from Fujii *et al.*'s F-actin model (the Fujii model)[10] and the chicken skeletal Tn core domain crystal structure (Protein Data Bank codes: 1YTZ and 1YV0)[6] were used. By systematically translating and rotating the Tn core domain around the F-actin filament, we obtained the best-fit models with and without Ca^{2+} by minimizing the squared sum of deviations of the calculated energy transfer efficiencies from the observed values for all of the FRET measurements at each orientation. Furthermore, we determined the location of Tm segment 167–195 on the F-actin filament, using the same procedures as previously reported[19] except that we used the coordinates from the Fujii model instead of the Lorenz model. Next, we constructed an atomic model of the Tn core domain–Tm (167–195)–F-actin complex with and without Ca^{2+}. The three-dimensional analysis of the FRET data herein provides a detailed model of the thin filament structure.

Results

We attached 5-(2-iodoacetylaminoethyl) amino-naphthalene 1-sulfonic acid (IAEDANS) to each cysteine in the single-cysteine TnC (E6C, E54C, S91C, R120C, E156C), TnI (A9C, T27C, Q41C, M57C, Q66C, D94C), and TnT25k mutants (A169C, S200C, Q217C, K230C, Q244C, S250C) as the energy donor molecule, 5-(((acetylamino)ethyl) amino)naphthalene-1-sulfonate (AEDANS) (IAEDANS after reaction with a sulfhydryl group). Each AEDANS-labeled Tn subunit was reconstructed into the Tn complex with additional Tn subunits. To examine whether the AEDANS-labeled Tn complex maintained native Tn activity, we measured Ca^{2+} regulation of actin-activated myosin subfragment 1 (S1)-ATPase activity for the labeled Tn complex (Fig. S1). Ca^{2+} sensitivity is defined as $[1 - (Activity_{-Ca}/Activity_{+Ca})] \times 100$. The labeled Tn complex exhibited approximately the same Ca^{2+} sensitivity as the native Tn (rabbit skeletal Tn). The relative Ca^{2+} sensitivity (percentage of native Tn sensitivity) for each AEDANS-

labeled Tn complex is shown in Table 1. IAEDANS was also attached to each cysteine in the single-cysteine Tm mutants at positions 167, 174, 181, 188, and 195. We measured Ca^{2+} regulation of actin-activated S1-ATPase activity for the labeled Tm mutants as we have previously reported,[19] and the relative Ca^{2+} sensitivity of each AEDANS-labeled Tm mutant is shown in Table 2. The energy acceptor molecules 4-dimethyl-aminophenylazophenyl 4′-maleimide (DABMI) and fluorescein cadaverine (FLC) were attached to actin Cys374 and Gln41, respectively, and the ADP bound to F-actin was replaced with 2′(or 3′)-O-(2,4,6-trinitrophenyl) (TNP)-ADP. Labeling F-actin with these acceptor probes did not impair Ca^{2+} sensitivity in the thin filaments.

FRET between the probes attached to Tn and the probes attached to F-actin on the reconstituted thin filament

The transfer efficiencies between AEDANS–Tn and FLC–F-actin were determined by measuring the donor fluorescence intensity with and without the acceptor. The solvent used for these experiments was buffer F [60 mM KCl, 2 mM $MgCl_2$, 20 mM Tris–HCl (pH 7.6), and 1 mM NaN_3] and either 50 μM $CaCl_2$ for the $+Ca^{2+}$ state or 1 mM ethylene glycol bis(β-aminoethyl ether) N,N'-tetraacetic acid for the $-Ca^{2+}$ state at 20 °C. The ratio of donor fluorescence quenching was measured by titrating AEDANS–Tn/Tm with FLC–F-actin with and without Ca^{2+}, as described by Miki *et al.*[20] The excitation wavelength was 340 nm. Although the donor fluorescence maximum was found to be 490 nm, emission was measured at 460 nm to avoid acceptor FLC emission. To correct for fluorescence intensity changes from either F-actin binding or dilution effects, we added the same amount of unlabeled F-actin to the AEDANS–Tn/Tm solution, and we took the ratio of the fluorescence intensities as the relative fluorescence intensity. The initial protein concentrations were 0.63 μM AEDANS–Tn and 0.67 μM Tm. FLC–F-actin absorption produced an inner-filter effect, which was corrected.[20,21] The relative fluorescence intensity decreased with an increase in the F-actin/Tn molar ratio up to 7:1 and was approximately constant with over 7-fold excess F-actin. The energy transfer efficiencies were obtained from saturation points. Two labeling ratios for the acceptor probes to F-actin (A/P) were used. The observed transfer efficiency (E_{obs}) and Förster's critical distance (R_0) for each donor–acceptor pair are shown in Table 1.

The FRET efficiencies between AEDANS–Tn and either DABMI-labeled F-actin (DAB–F-actin) or TNP-ADP–F-actin were determined by measuring the donor fluorescence intensity as described for FLC–F-actin. The AEDANS emission was measured at 490 nm; DAB–F-actin and TNP-ADP–F-actin do not fluoresce. Furthermore, the transfer efficiencies were determined using a time-resolved single-photon counting method; contaminating emission from the acceptor was entirely avoided and a sufficient donor emission signal was obtained. Typical fluorescence decay curves for AEDANS–Tn with and without the acceptor (DAB) in the reconstituted thin filament are shown in Fig. S2.

The transfer efficiencies were determined by the lifetime-weighted quantum yield ($\langle\tau\rangle = \Sigma\ \alpha_i\tau_i$) with the acceptor ($\langle\tau\rangle_{DA}$) and without the acceptor ($\langle\tau\rangle_{D0}$).[21] These transfer efficiency values were similar (within 10%) to those determined by fluorescence intensity measurements using a steady-state fluorometer. Because the lifetime measurements are unaffected by either a change in donor concentration between samples or inner-filter effects, the transfer efficiencies determined by lifetime-weighted quantum yield were used herein for FRET between AEDANS–Tn and either DAB–F-actin or TNP-ADP–F-actin. For FRET between the probes attached to F-actin monomers, the relationship between the transfer efficiency and the acceptor ratio (labeling ratio) depends on the radial coordinates of the donor and acceptor positions in the thin filament. The FRET measurements using different acceptor labeling ratios provide information on the radial coordinates of the donor and acceptor. Therefore, to increase the accuracy in locating the Tn core domain on F-actin, we measured the transfer efficiencies at different acceptor labeling ratios (two) as described by Miki *et al.*[19] The E_{obs} values are summarized in Table 1.

Positioning the Tn core domain with Ca^{2+} on F-actin in the reconstituted thin filament

First, we attempted to place the atomic structure of the Tn core domain on the F-actin filament using 102 E_{obs} values with Ca^{2+} (Table 1). The atomic coordinates from the Fujii model (composed of 11 actin monomers) and the Tn core domain with Ca^{2+} (1YTZ) were used. The C^{α} and C^{γ} coordinates for the labeled amino acid residues in the Tn core domain and actin (the O2′ atom of bound ADP for TNP-ADP), respectively, were used as the labeled positions. The difference in residue numbering between the chicken skeletal Tn and the rabbit skeletal Tn was taken into consideration. The residue numbers E6, E54, S91, R120, and E156 of the rabbit skeletal TnC were assigned to 8, 56, 93, 122, and 158 of the chicken skeletal TnC, respectively; the residue numbers 9, 27, 41, 57, 66, and 94 of the rabbit skeletal TnI were the same as the chicken skeletal TnI, and the residue numbers 169, 200, 217, 230, 244, and 250 of

Table 1. FRET between Tn and F-actin on the reconstituted thin filament

Tn (D)	Q_0 (+Ca), Q_0 (−Ca)	Actin (A)	R_0 (+Ca), R_0 (−Ca)	A/P	E_{obs}/E_{calc}(A)/E_{calc}(B) +Ca^{2+}	−Ca^{2+}
T169 (102%)	0.266, 0.289	DAB	37.4, 37.9	0.75	0.39/0.49/0.50	0.51/0.79/0.79
				1.00	0.49/0.59/0.60	0.62/0.99/0.88
		TNP	38.1, 38.6	0.44	0.38/0.48/0.33	0.45/0.48/0.35
				0.58	0.43/0.53/0.43	0.51/0.58/0.43
		FLC	44.3, 44.9	0.70	0.51/0.74/0.72	0.57/0.80/0.82
				0.89	0.66/0.83/0.85	0.73/0.93/0.93
T200 (103%)	0.300, 0.294	DAB	38.1, 38.0	0.75	0.32/0.16/0.16	0.31/0.06/0.07
				1.00	0.35/0.21/0.20	0.34/0.09/0.10
		TNP	38.9, 38.7	0.44	0.31/0.17/0.29	0.29/0.04/0.02
				0.58	0.31/0.22/0.37	0.29/0.05/0.02
		FLC	45.2, 45.1	0.74	0.28/0.35/0.34	0.21/0.15/0.11
				0.98	0.29/0.43/0.42	0.27/0.19/0.14
T217 (92%)	0.209, 0.207	DAB	35.9, 35.9	0.75	0.13/0.07/0.08	0.20/0.09/0.12
				1.00	0.26/0.09/0.10	0.31/0.11/0.16
		TNP	36.6, 36.5	0.44	0.10/0.13/0.15	0.16/0.09/0.05
				0.58	0.12/0.16/0.19	0.13/0.12/0.06
		FLC	42.6, 42.5	0.74	0.37/0.25/0.25	0.44/0.28/0.20
				0.98	0.47/0.31/0.31	0.55/0.35/0.26
T230 (97%)	0.312, 0.311	DAB	38.4, 38.4	0.75	0.26/0.12/0.12	0.39/0.27/0.29
				1.00	0.33/0.15/0.15	0.42/0.34/0.36
		TNP	39.1, 39.1	0.44	0.23/0.19/0.20	0.26/0.40/0.29
				0.58	0.23/0.24/0.25	0.31/0.50/0.36
		FLC	45.5, 45.5	0.74	0.32/0.29/0.31	0.41/0.60/0.53
				0.98	0.54/0.35/0.38	0.68/0.72/0.62
T244 (111%)	0.263, 0.287	DAB	37.3, 37.9	0.75	0.37/0.30/0.27	0.49/0.50/0.47
				1.00	0.49/0.39/0.35	0.64/0.60/0.57
		TNP	38.0, 38.6	0.44	0.37/0.26/0.22	0.48/0.54/0.56
				0.58	0.40/0.33/0.29	0.52/0.68/0.69
		FLC	44.2, 44.9	0.70	0.50/0.39/0.46	0.59/0.76/0.73
				0.89	0.63/0.47/0.55	0.74/0.82/0.80
T250 (91%)	0.295, 0.318	DAB	38.0, 38.5	0.75	0.35/0.50/0.45	0.55/0.59/0.61
				1.00	0.45/0.62/0.57	0.70/0.68/0.70
		TNP	38.8, 39.2	0.44	0.32/0.31/0.26	0.48/0.60/0.59
				0.58	0.36/0.39/0.33	0.54/0.73/0.72
		FLC	45.1, 45.7	0.74	0.47/0.59/0.69	0.56/0.86/0.85
				0.98	0.63/0.68/0.85	0.76/0.92/0.90
I9 (95%)	0.248, 0.245	DAB	36.9, 36.9	0.75	0.05/0.04/0.03	0.13/0.17/0.12
				1.00	0.11/0.06/0.04	0.18/0.22/0.16
		TNP	37.6, 37.6	0.40	0.05/0.03/0.03	0.11/0.15/0.20
				0.64	0.08/0.05/0.05	0.20/0.23/0.31
		FLC	43.8, 43.7	0.74	0.12/0.09/0.09	0.19/0.29/0.30
				0.98	0.29/0.12/0.12	0.39/0.36/0.38
I27 (94%)	0.248, 0.247	DAB	37.0, 36.9	0.75	0.15/0.03/0.03	0.25/0.07/0.07
				1.00	0.18/0.04/0.04	0.27/0.09/0.09
		TNP	37.7, 37.6	0.44	0.12/0.05/0.05	0.17/0.14/0.12
				0.58	0.14/0.06/0.07	0.19/0.19/0.16
		FLC	43.8, 43.8	0.74	0.26/0.09/0.09	0.28/0.20/0.19
				0.98	0.39/0.11/0.12	0.45/0.25/0.24
I41 (97%)	0.201, 0.210	DAB	35.7, 35.9	0.75	0.04/0.03/0.03	0.06/0.07/0.10
				1.00	0.05/0.04/0.05	0.12/0.09/0.13
		TNP	36.3, 36.6	0.44	0.00/0.05/0.06	0.04/0.10/0.07
				0.58	0.00/0.07/0.08	0.06/0.14/0.09
		FLC	42.3, 42.6	0.70	0.10/0.10/0.11	0.18/0.21/0.18
				0.89	0.18/0.12/0.13	0.24/0.26/0.23
I57 (105%)	0.232, 0.231	DAB	36.5, 36.5	0.75	0.07/0.08/0.07	0.12/0.08/0.10
				1.00	0.13/0.10/0.09	0.15/0.11/0.13
		TNP	37.2, 37.2	0.44	0.10/0.11/0.14	0.09/0.05/0.02
				0.58	0.11/0.14/0.19	0.11/0.07/0.03
		FLC	43.3, 43.3	0.74	0.17/0.20/0.18	0.19/0.17/0.13
				0.98	0.24/0.26/0.23	0.28/0.22/0.17
I66 (97%)	0.195, 0.209	DAB	35.5, 35.9	0.75	0.09/0.07/0.07	0.12/0.15/0.28
				1.00	0.14/0.09/0.09	0.18/0.19/0.36
		TNP	36.2, 36.6	0.44	0.10/0.16/0.13	0.13/0.14/0.05
				0.58	0.10/0.20/0.17	0.07/0.18/0.06
		FLC	42.1, 42.6	0.70	0.20/0.21/0.21	0.25/0.35/0.30
				0.89	0.31/0.26/0.26	0.35/0.42/0.36

Table 1 (*continued*)

Tn (D)	Q_0 (+Ca), Q_0 (−Ca)	Actin (A)	R_0 (+Ca), R_0 (−Ca)	A/P	$E_{obs}/E_{calc}(A)/E_{calc}(B)$ +Ca^{2+}	−Ca^{2+}
I94 (92%)	0.296, 0.304	DAB	38.1, 38.2	0.75	0.43/0.35/0.39	0.53/0.58/0.56
				1.00	0.56/0.44/0.49	0.69/0.73/0.69
		TNP	38.8, 39.0	0.40	0.27/0.41/0.40	0.29/0.46/0.41
				0.61	0.49/0.60/0.58	0.57/0.66/0.57
		FLC	45.1, 45.3	0.74	0.52/0.58/0.62	0.64/0.77/0.68
				0.98	0.63/0.67/0.72	0.78/0.88/0.76
C6 (103%)	0.280, 0.275	DAB	37.7, 37.6	0.75	0.21/0.10/0.12	0.29/0.07/0.07
				1.00	0.28/0.13/0.16	0.35/0.09/0.09
		TNP	38.4, 38.3	0.44	0.21/0.22/0.21	0.30/0.13/0.14
				0.58	0.24/0.28/0.27	0.33/0.17/0.18
		FLC	44.7, 44.6	0.74	0.16/0.31/0.30	0.24/0.20/0.20
				0.98	0.31/0.39/0.37	0.38/0.25/0.26
C54 (92%)	0.309, 0.292	DAB	38.3, 38.0	0.75	0.32/0.40/0.40	0.24/0.19/0.25
				1.00	0.43/0.50/0.49	0.31/0.24/0.32
		TNP	39.0, 38.7	0.44	0.31/0.46/0.51	0.32/0.25/0.20
				0.58	0.35/0.59/0.64	0.38/0.33/0.25
		FLC	45.4, 45.0	0.74	0.43/0.65/0.65	0.25/0.41/0.36
				0.98	0.63/0.74/0.73	0.46/0.49/0.45
C91 (108%)	0.308, 0.276	DAB	38.3, 37.6	0.75	0.18/0.09/0.09	0.24/ND/ND
				1.00	0.22/0.12/0.12	0.32/ND/ND
		TNP	39.0, 38.3	0.44	0.15/0.18/0.19	0.23/ND/ND
				0.58	0.15/0.23/0.24	0.27/ND/ND
		FLC	45.4, 44.6	0.70	0.25/0.22/0.24	0.28/ND/ND
				0.89	0.32/0.26/0.29	0.33/ND/ND
C120 (98%)	0.286, 0.279	DAB	37.8, 37.7	0.75	0.29/0.03/0.03	0.33/0.17/0.11
				1.00	0.32/0.04/0.04	0.32/0.22/0.14
		TNP	38.5, 38.4	0.44	0.32/0.03/0.03	0.32/0.21/0.22
				0.58	0.30/0.04/0.04	0.30/0.27/0.28
		FLC	44.9, 44.7	0.74	0.12/0.12/0.08	0.16/0.32/0.34
				0.98	0.26/0.10/0.11	0.29/0.39/0.42
C156 (95%)	0.273, 0.249	DAB	37.6, 37.0	0.75	0.16/0.09/0.08	0.25/0.15/0.13
				1.00	0.23/0.11/0.10	0.34/0.19/0.17
		TNP	38.3, 37.7	0.44	0.16/0.14/0.13	0.31/0.33/0.33
				0.58	0.19/0.18/0.17	0.35/0.42/0.43
		FLC	44.5, 43.8	0.70	0.30/0.19/0.22	0.34/0.33/0.33
				0.89	0.46/0.24/0.27	0.50/0.39/0.39

In the leftmost column, the percentage denoted beside the Tn residue number shows relative Ca^{2+} sensitivity (100% for native Tn). Q_0, the quantum yield of AEDANS attached to the Tn subunit on the reconstituted thin filament in the presence of Ca^{2+} (+Ca) and in the absence of Ca^{2+} (−Ca); R_0, Förster's critical distance (in angstroms) in the presence of Ca^{2+} (+Ca) and in the absence of Ca^{2+} (−Ca); A/P, acceptor/protein (actin) labeling ratio; E_{obs}, measured energy transfer efficiency (errors in E_{obs} were within ±0.03); $E_{calc}(A)$ and $E_{calc}(B)$, calculated energy transfer efficiency at two best-fit models, A-model and B-model, respectively.

the rabbit skeletal TnT were assigned to 167, 198, 215, 228, 242, and 248 of the chicken skeletal TnT, respectively. The long axis of F-actin was aligned along the *z*-axis from the barbed end to the pointed end, and the *z*-axis value was set to zero for the contact surface between the fifth actin monomer and the seventh actin monomer. The *x*-axis was set along the contact surface between the fifth actin monomer and the sixth actin monomer. The center of the coordinates for the 17 C$^{\alpha}$ atoms from the labeled amino acid residues in the Tn core domain was placed at *Z* on the *z*-axis. The radius for the Tn core domain bound to actin was defined as *R*. The Tn core domain azimuth (the angle from the *x*-axis on an *X*–*Y* plane) was defined as ϕ. Eulerian angles, α, β, and γ, were employed to describe the rotational parameters around the center of the Tn core domain. Figure 1 shows the spatial parameters (*R*, *Z*, and ϕ) that describe the Tn core domain position on the F-actin filament.

The possible arrangements for the Tn core domain on F-actin were explored by systematically changing the values of the six spatial parameters such that all possible orientations were analyzed. At each orientation, the distances between each donor and the acceptors on 11 actin monomers were calculated from the coordinates for each FRET pair. Because transfer efficiency is a function of the inverse of the sixth power of the distance between the donor and the acceptor, a calculation with greater than five acceptors is unnecessary. The five nearest-neighbor distances were used to calculate the FRET efficiency, as previously analyzed for locating Tm on F-actin.[19] Using these distance values, we calculated the energy transfer efficiency (E_{calc}) for each FRET pair

Table 2. FRET between Tm segment 167–195 and F-actin on the reconstituted thin filament

					E_{obs}/E_{calc}	
Tm (D)	Q_0 (+Ca), Q_0 (−Ca)	Actin (A)	R_0 (+Ca), R_0 (−Ca)	A/P	+Ca^{2+}	−Ca^{2+}
*167 (99%)	0.285, 0.275	DAB	37.8, 37.6	0.50	0.26/0.20	0.27/0.19
				1.00	0.41/0.34	0.42/0.33
		TNP	38.5, 38.3	0.40	0.33/0.30	0.33/0.31
				0.60	0.38/0.41	0.38/0.42
		FLC	44.8, 44.6	0.49	0.37/0.39	0.37/0.39
				0.96	0.42/0.59	0.42/0.59
*174 (104%)	0.252, 0.263	DAB	36.7, 37.1	0.50	0.27/0.20	0.30/0.21
				1.00	0.40/0.36	0.43/0.36
		TNP	37.4, 37.8	0.40	0.31/0.30	0.36/0.32
				0.60	0.50/0.42	0.55/0.46
		FLC	43.6, 44.0	0.49	0.38/0.35	0.38/0.37
				0.96	0.45/0.53	0.45/0.56
181 (90%)	0.251, 0.246	DAB	37.1, 37.7	0.50	0.27/0.25	0.28/0.26
				1.00	0.46/0.45	0.50/0.47
		TNP	37.8, 38.4	0.45	0.41/0.35	0.48/0.39
				0.61	0.45/0.46	0.52/0.51
		FLC	44.0, 44.7	0.61	0.37/0.42	0.39/0.45
				0.88	0.54/0.53	0.56/0.56
188 (98%)	0.298, 0.299	DAB	37.0, 37.1	0.50	0.25/0.24	0.26/0.26
				1.00	0.44/0.45	0.48/0.47
		TNP	37.7, 37.8	0.45	0.41/0.34	0.43/0.37
				0.61	0.46/0.44	0.49/0.48
		FLC	43.8, 44.0	0.61	0.34/0.44	0.36/0.46
				0.88	0.46/0.56	0.50/0.58
195 (85%)	0.294, 0.300	DAB	37.5, 37.3	0.50	0.32/0.25	0.34/0.26
				1.00	0.51/0.45	0.55/0.48
		TNP	38.2, 38.0	0.45	0.37/0.30	0.39/0.32
				0.61	0.41/0.39	0.43/0.41
		FLC	44.5, 44.3	0.61	0.41/0.48	0.42/0.49
				0.88	0.59/0.61	0.63/0.62

In the leftmost column, the percentage denoted beside the Tm residue number shows relative Ca^{2+} sensitivity (100% for native Tm). Q_0, the quantum yield of AEDANS attached to Tm on the reconstituted thin filament in the presence of Ca^{2+} (+Ca) and in the absence of Ca^{2+} (−Ca); R_0, Förster's critical distance (in angstroms); A/P, acceptor/protein (actin) labeling ratio; E_{obs}, measured energy transfer efficiency (errors in E_{obs} were within ±0.03); E_{calc}, calculated transfer efficiency at the best-fit model. Data in *167 and *174 except E_{calc} values are used from our previous report by Miki *et al.*[19]

at the acceptor-labeling ratio according to Eqs. (2)–(8). At each orientation, the squared sum (*Res*) of deviations of the calculated energy transfer efficiencies from the observed values (E_{obs}) for all FRET pairs was calculated as follows:

$$Res= \sum_{\text{data set}} (E_{obs} - E_{calc})^2 \qquad (1)$$

At the fixed values of R, Z, and ϕ (initial values), every Eulerian angle parameter in a 10° grid ($0° \leq \alpha \leq 360°$, $0° \leq \beta \leq 180°$, and $0° \leq \gamma \leq 360°$) was searched and the minimum value of the residuals was obtained. Next, ϕ was changed from 0° to 180° with a step size of 5°. At each ϕ value, every Eulerian angle parameter in a 10° grid was searched, and the minimum value of the residuals was obtained. Z was then changed from −28 Å to +28 Å with a step size of 4 Å. At each Z value, the ϕ, α, β, and γ values were changed as described above such that the minimum value of the residuals was obtained. Finally, R was changed from 45 Å to 70 Å with a step size of 5 Å (2 Å over the 56- to 62-Å range). At each R value, the Z, ϕ, α, β, and γ values were systematically changed. Thus, the global minimum of residuals was obtained. We determined the minimum values of the residual for each R and Z value. The three-dimensional map of the residuals as a function of R and Z is shown in Fig. S3. Two nearly equal minimum values were obtained at different orientations. Next, we searched for the refined global minimum by using smaller grids of spatial parameters ($\Delta\alpha = \Delta\beta = \Delta\gamma = 5°$, $\Delta\phi = 2°$, $\Delta Z = 2$ Å, and $\Delta R = 1$ Å) near the ranges for the two minimum values. We obtained two minimum values of the residuals for the spatial parameters $R = 58$ Å, $Z = −6$ Å, $\phi = 72°$, $\alpha = 335°$, $\beta = 130°$, and $\gamma = 135°$ (A-model) as well as $R = 58$ Å, $Z = +6$ Å, $\phi = 90°$, $\alpha = 135°$, $\beta = 25°$, and $\gamma = 40°$ (B-model). The root-mean-square errors between the calculated transfer efficiencies and the observed values were both 0.119. Figure 2 shows the A- and B-models. Comparisons of the individual FRET efficiencies for the best-fit models to the observed data are shown in Table 1.

(a) **(b)**
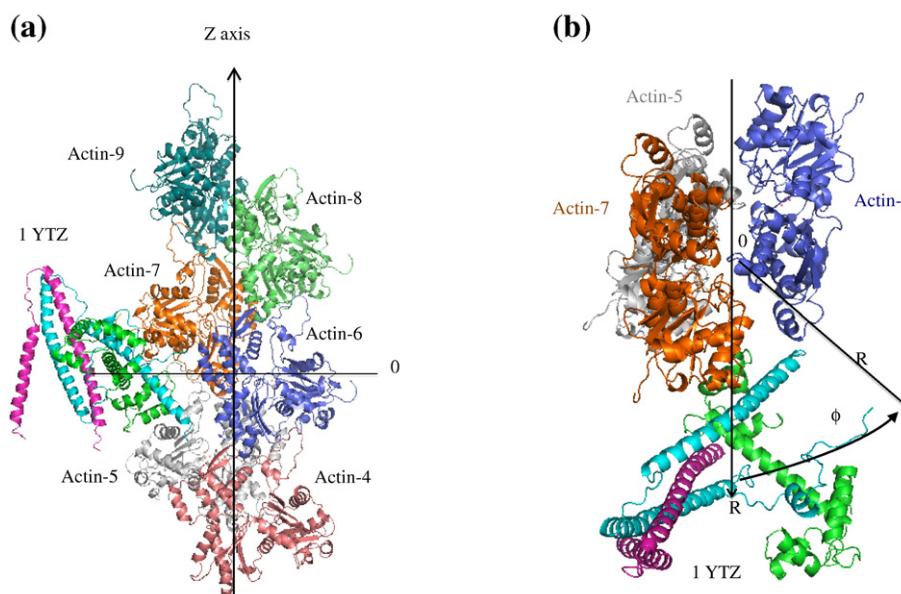
Fig. 1. The Tn core domain (1YTZ) was positioned on F-actin with the six spatial parameters [Z, R, ϕ, and three Eulerian angles (α, β, and γ)] used to search for all possible orientations. For the calculations, the coordinates of the 11 actin monomers were used. (a) View along the F-actin axis. Only the fourth actin monomer up to the ninth actin monomer are shown here. (b) View from the pointed end. Only the fifth actin monomer up to the seventh actin monomer are shown here.

Positioning the Tn core domain without Ca^{2+} on F-actin in the reconstituted thin filament

Because the atomic coordinates for TnC residue 91 are missing from the Tn core domain without Ca^{2+} (1YV0), we searched for the orientation and location of 1YV0 on the F-actin filament using 96 E_{obs} values without Ca^{2+} (Table 1), according to the same procedure described for 1YTZ. The three-dimen-

sional map of the residuals as a function of R and Z is shown in Fig. S3. As seen for 1YTZ, two approximately equal minimum values were obtained at different orientations. Then, we searched for the refined global minimum using smaller spatial parameter grids ($\Delta\alpha = \Delta\beta = \Delta\gamma = 5°$, $\Delta\phi = 2°$, $\Delta Z = 2$ Å, and $\Delta R = 1$ Å) near the two minimum value ranges. We obtained two minimum values of the residuals for the spatial parameters $R = 54$ Å,

(a) **(b)**
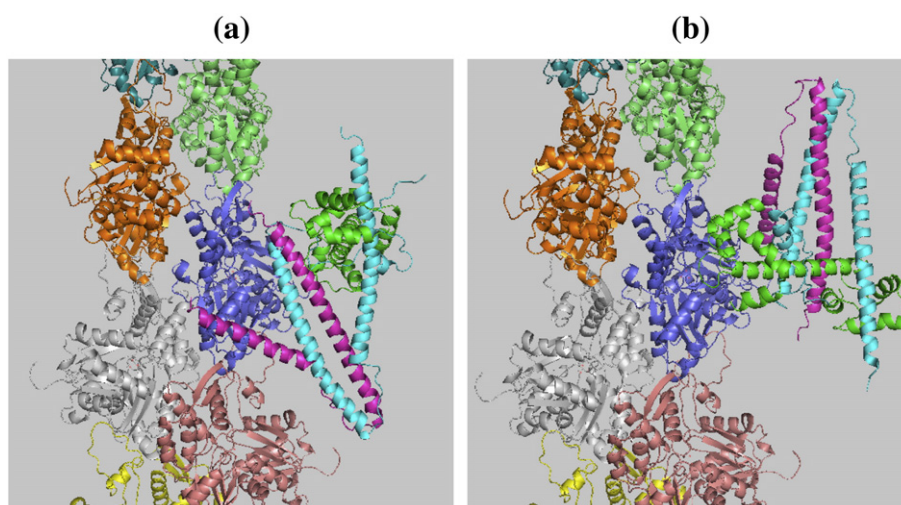
Fig. 2. The two best-fit models (a and b) for the Tn core domain (1YTZ) and the F-actin complex with Ca^{2+}. Tn subunits C, I, and T are colored green, cyan, and magenta, respectively.

$Z = -12$ Å, $\phi = 84°$, $\alpha = 90°$, $\beta = 120°$, and $\gamma = 95°$ (A-model) as well as $R = 54$ Å, $Z = +20$ Å, $\phi = 64°$, $\alpha = 290°$, $\beta = 65°$, and $\gamma = 75°$ (B-model). The root-mean-square errors between the calculated transfer efficiencies and the observed values were both 0.132. Figure 3 shows the A- and B-models.

Positioning Tm segment 167–195 on F-actin in the reconstituted thin filament with and without Ca^{2+}

As we reported previously,[19] we generated five single-cysteine mutants at positions 167, 174, 181, 188, and 195 in the 167–195 region of rabbit skeletal muscle α-Tm to locate the Tm segment 167–195 on F-actin. The energy donor probe IAEDANS was attached to each of the single-cysteine mutants. The FRET efficiencies between the energy donor probe AEDANS attached to Tm and either the energy acceptor probe FLC, DAB, or TNP-ADP attached to F-actin were determined with and without Ca^{2+} as previously reported for methods with similar procedures for FRET measurements between AEDANS–Tn and either FLC–F-actin, DAB–F-actin, or TNP-ADP–F-actin. The E_{obs} values are summarized in Table 2 in which the E_{obs} values for Tm167 and Tm174 are cited from our previous report.[19]

We searched for the orientation of the Tm segment 167–195 on F-actin, using the same procedures as we previously reported[19] for constructing an atomic model of the actin–Tm complex on a reconstituted thin filament. Herein, the atomic coordinates for the Fujii model (composed of 11 actin monomers), instead of the Lorenz model, were used to construct the atomic model. The C$^{\beta}$ and C$^{\gamma}$ coordinates for the labeled amino acid residues in Tm and actin (the O2′ atom for TNP-ADP), respectively, were used as the labeled positions. Tm segment 167–195 was aligned along the z-axis from its C-terminus to its N-terminus, and the center of the coordinates for the two C$^{\beta}$ atoms of residue 181 in the two Tm chains was placed at Z ($Z = -28$ Å to $+28$ Å, $\Delta Z = 1$ Å) on the z-axis as shown in Fig. 1. The angle between the Tm segment's long axis and the z-axis was defined as θ ($\theta = -4°$ to $-32°$, $\Delta\theta = 1°$). The radius of the Tm segment bound to actin was defined as R ($R = 38$–44 Å, $\Delta R = 1$ Å). The Tm azimuth (angle from the x-axis on an X–Y plane) was defined as ϕ ($\phi = 0$–$180°$, $\Delta\phi = 2°$). The rotational angle around the Tm axis was defined as ψ ($\psi = 0$–$360°$, $\Delta\psi = 5°$). By changing these five spatial parameters, we searched all possible arrangements for the Tm segment on F-actin to calculate the FRET efficiencies for each donor–acceptor pair in each arrangement. By minimizing the squared sum of deviations for the calculated FRET efficiencies from the observed FRET efficiencies, we determined the location of the Tm segment on the F-actin filament. The global minimums of the residuals were obtained at $R = 42$ Å, $\theta = 28°$, $Z = +6$ Å, $\phi = 54°$, and $\psi = 310°$ for the $+$Ca^{2+} state with a root-mean-square error of 0.060 and at $R = 41$ Å, $\theta = 26°$, $Z = +8$ Å, $\phi = 56°$, and $\psi = 315°$ for the $-$Ca^{2+} state with a root-mean-square error of 0.068. Comparisons of the individual FRET efficiencies for the best-fit models of the observed data are presented in Table 2. The best-fit models of the Tm segment 167–195 and F-actin complex with and without Ca^{2+} are shown in Fig. 4.

Discussion

Using 102 FRET efficiencies with Ca^{2+} and 96 FRET efficiencies without Ca^{2+} as restraints, we determined the location of the Tn core domain (1YTZ with Ca^{2+} and 1YV0 without Ca^{2+}) on the F-actin filament, since the atomic coordinates of TnC-Ser91 (Ser93 in the chicken skeletal muscle
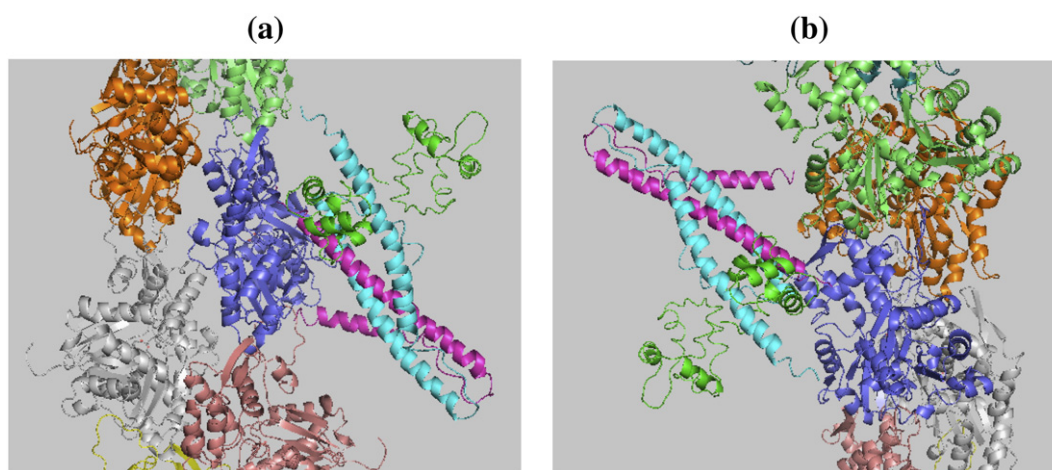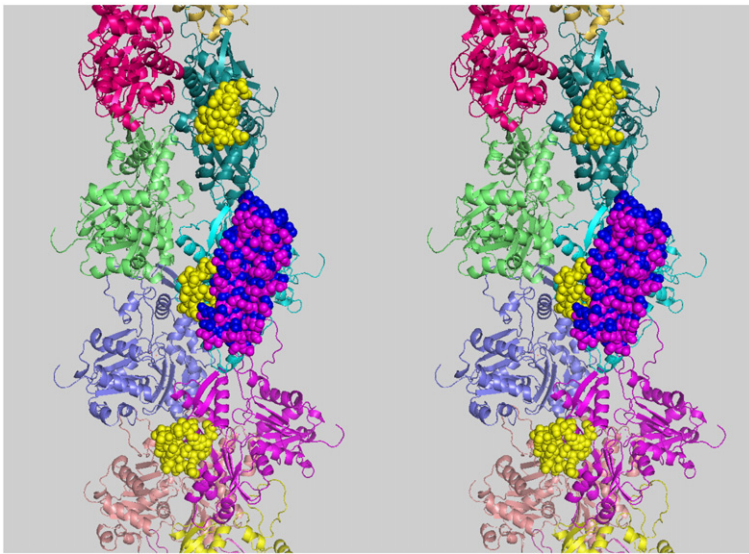
(a)   **(b)**

Fig. 3. The two best-fit models (a and b) for the Tn core domain (1YV0) and the F-actin complex without Ca^{2+}.

Fig. 4. Stereo views of the best-fit models for the Tm (167–195) and F-actin complex. The Tm segments are shown in magenta and blue with and without Ca^{2+}, respectively. The Tm binding region (217–236) proposed by Flaherty *et al.*[22] is represented by yellow spheres.

TnC) are missing in 1YV0. Herein, we evaluate the models by comparing them with other biochemical and structural studies on Tn, Tm, and the thin filament. By searching the minimum value of residuals for all possible orientations and locations of the Tn core domain on F-actin, we obtained two models with different orientations (Figs. 2 and 3). In the A-model, the arrowhead-shaped I–T complex points toward the barbed end of the F-actin, but in the B-model, the direction is reversed. In our previous report,[18] we constructed an atomic model of the Tn–Tm complex on a reconstituted thin filament in which the arrowhead-shaped I–T complex pointed toward the barbed end of F-actin as shown in the A-model. Therefore, and hereafter, we

adopt the A-model. Figure 5 shows the stereo views for the best-fit models of F-actin and the Tn core domain with and without Ca^{2+}. The model shows that the bulk of the Tn core domain is located near actin subdomains 3 and 4 with the TnC N-terminal domain directed toward actin subdomain 2. After Ca^{2+} release, the Tn core domain moves closer to the center of the F-actin axis by ~ 4 Å and toward the actin outer domain. On the other hand, the polarized fluorescence from bifunctional rhodamine probes on the C and E helices of TnC in the muscle fiber was used to orient the Tn core domain structure in the fiber by Sun *et al.*[23] They showed that the I–T arm is 30° to the filament axis in active muscle, and it tilts to $\sim 40°$ in relaxed muscle, which allows the regulatory
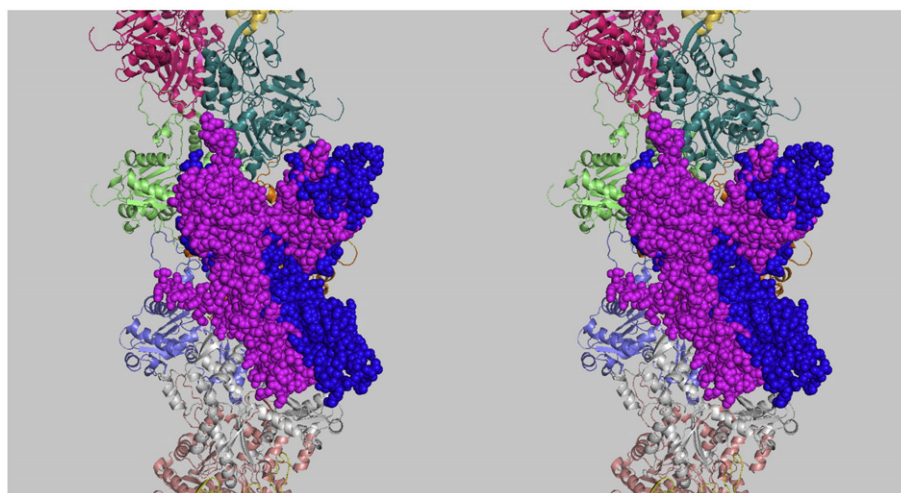
Fig. 5. Stereo views of the best-fit models for the Tn core domain (A-models with and without Ca^{2+}) and F-actin complex. The Tn core domains, 1YTZ and 1YV0, are represented by magenta and blue spheres, respectively.

head to tilt through a larger angle. In their model, the angle between the TnC central helix and the actin filament axis is ∼70° with Ca^{2+} and ∼55° without Ca^{2+}. In our model herein, the angle between the I–T arm and the actin filament axis is ∼30° with Ca^{2+} and ∼40° without Ca^{2+}, and the angle between the TnC central helix and the actin filament is ∼70° with Ca^{2+} and ∼60° without Ca^{2+}, which agrees with the results of Sun *et al.*[23] Although FRET was measured in a randomly oriented solution, FRET yielded the same orientation for the Tn core domain on F-actin as polarized fluorescence measurements in which the filament must be uniformly oriented. Thus, FRET methods have many advantages compared with other biophysical methods: provision of information about the thin filament structure in the physiological solution and absence of need to orient the filament direction uniformly. Furthermore, energy donor and energy acceptor probes are specifically attached to proteins, so that assigning a factor to conformational change is obvious. Among the structural models derived from 3D-EM and X-ray diffraction measurements,[11–15] the orientation of the Tn core domain on the F-actin filament from Lehman's group[13,15] is very similar to our model, although the positions of Tm and the Tn core domain on the F-actin filament with and without Ca^{2+} are substantially different from our model.

Our previous model of the Tn–Tm complex[18] also suggested that the Tn core domain is located at the 160–208 region of Tm. To construct an atomic model of the Tn core domain, Tm, and F-actin complex, we positioned the atomic structure of Tm segment 167–195 on the F-actin filament with and without Ca^{2+}. In our previous report,[19] we used the atomic coordinates for the Lorenz model to localize each of the five Tm regions 41–69, 83–111, 146–174, 216–244, and 252–236 on F-actin in a reconstituted thin filament. For the studies herein, we used the atomic coordinates for the Fujii model instead of the Lorenz model. Using the same procedures, we determined the segment's location on F-actin. Figure 4 shows that the 167–195 region of Tm is proximal to the actin residues 217–236, which compose the Tm binding site according to Flaherty *et al.*[22] Tm contains seven quasi-equivalent periods and spans seven actin monomers. Tm period 5 comprises 166–207 residues. Figure 4 shows that residue 167 is located at the contact region between actin monomers along the long-pitch helix of F-actin, which indicates that each Tm period covers an actin monomer. These localization features for Tm on F-actin agree with our previous model calculated using the atomic coordinates for the Lorenz model.

Figure 6 shows the stereo views for the best-fit models of the Tn core domain, Tm segment 167–195, and F-actin complex with Ca^{2+}. This model localizes the C-terminal region of TnT close to Tm, which was

reported to compose the Tm binding site.[24] The model shows that the C-terminal region of the Tn I–T arm appears to form a helix bundle with Tm 179–189, although the space between the TnI– and the TnT–C-terminal helices in the I–T arm is insufficient to form the helix bundle. In the model, the TnT2–N-terminal helix [H1(T2)] intrudes into the space between actin and Tm, which is improbable. There are two crystal structures of the Tn core domain: human cardiac Tn[5] and chicken skeletal Tn.[6] Superposition of these Tn structures in the Ca^{2+}-saturated state shows that the direction and the length of the TnT2–N-terminal helix are different, although the overall organization of the subunits is similar. It is likely that the *in situ* conformation of the Tn core domain is significantly different from the crystal structures in the space between the TnI– and TnT–C-terminal helices in the I–T arm as well as the direction and the length of the TnT2–N-terminal helix. It has been reported that Ala clusters are associated with bends or staggers and a reduced interchain distance in the Tm crystal structures.[25,26] In wild-type Tm, the only periodic actin binding motifs that contain destabilizing interface Ala (Ala clusters) are periods 1 (amino acids 18–22–25) and 5 (179–183–186).[27] The helix bundle formation for Tm region 179–189 and the Tn I–T arm C-terminal region suggests that Tn easily affects the Tm conformation through this flexible Ala cluster region, which is important for muscle regulation.

In the FRET analysis, due to the ambiguity in the value of the dipole–dipole orientation factor between the energy donor and acceptor molecules and the dimensions of the probes attached through linkers to the residue side chains, the measured distance has a ±10% uncertainty.[16] However, although the length of the probe linkers is ∼10 Å, the linker does not extend uni-directionally, but it folds randomly. For a single donor and multiple acceptors as in the FRET experiments herein, the directions for linker extension are further randomized. Because the atomic coordinates for the amino acid residues but not the probes are available for the model construction herein, we cannot directly evaluate the ambiguity derived from the linker lengths. However, in our previous report in which we constructed an atomic model of the actin–Tm complex on a reconstituted thin filament, we used the C^{α} and C^{γ} coordinates, instead of the C^{β} coordinates, of the labeled amino acid Tm residues as the labeled positions. The best-fit models were approximately the same, suggesting that the length of the probe linker does not significantly affect the model construction. For the present analysis, we used the atomic coordinates from the Fujii model, instead of the Lorenz model. Herein, we used the atomic coordinates from the Lorenz model to locate the Tn core domain and Tm segment 167–195 according to the same procedures as discussed in
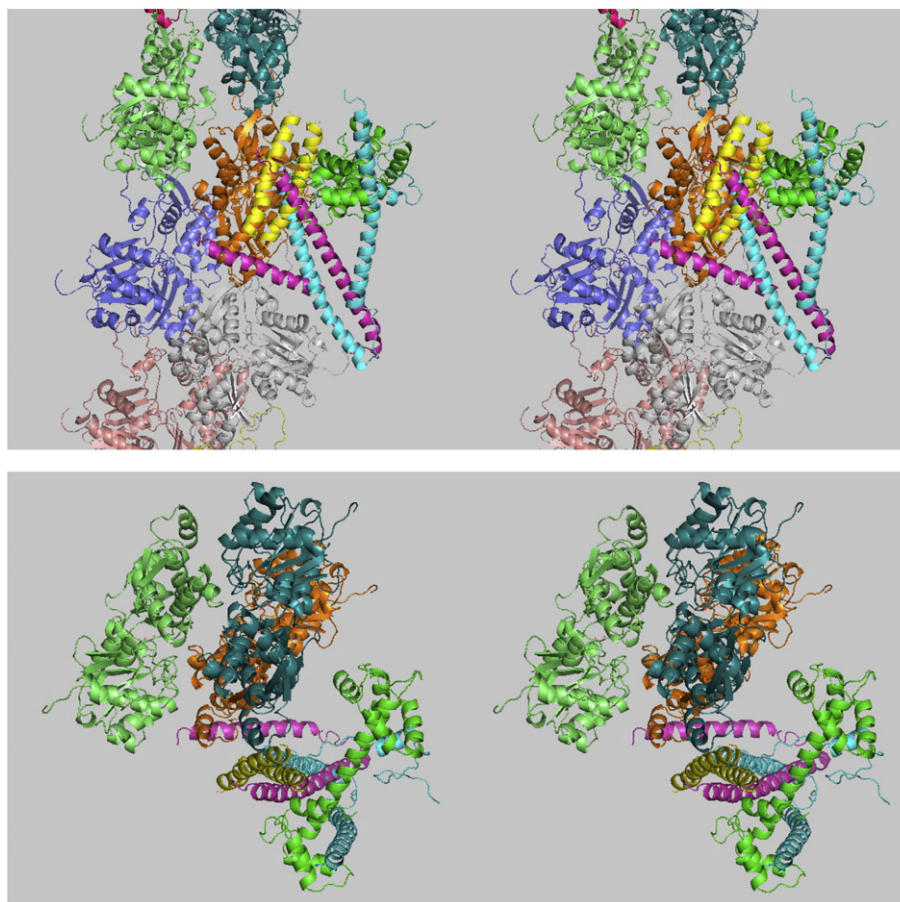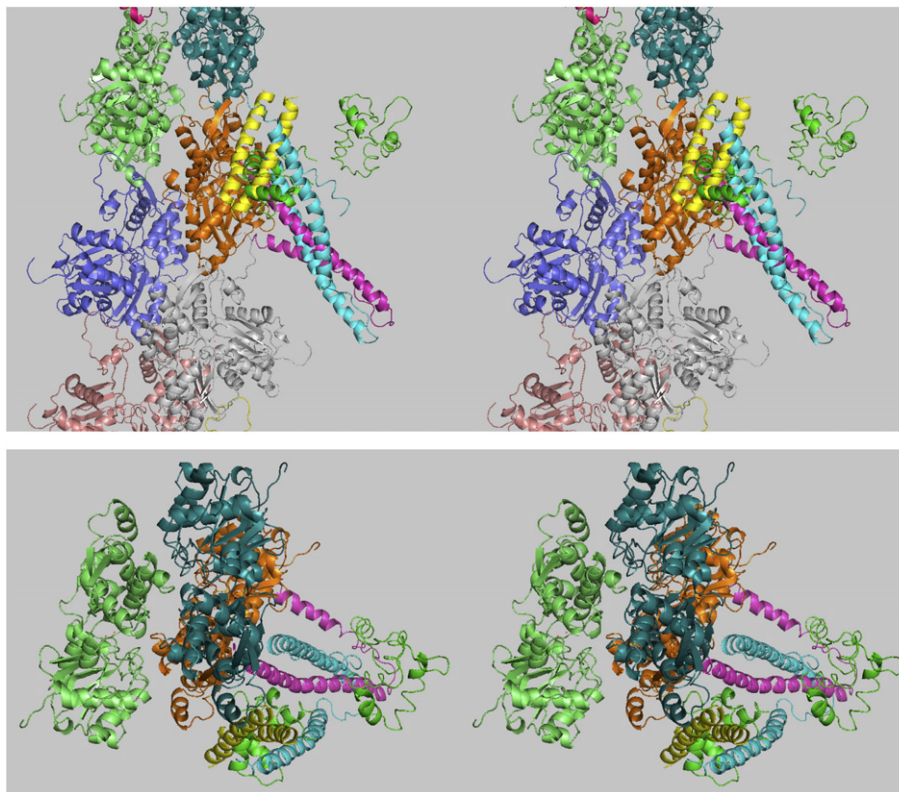
Fig. 6. Stereo views of the best-fit model for the Tn core domain, Tm segment (167–195), and F-actin complex with Ca^{2+}. The Tn subunits C, I, and T are colored green, cyan, and magenta, respectively, and Tm segment 167–195 is colored yellow. The top figure shows the view along the F-actin axis, and the bottom figure shows the view from the pointed end. Only the fifth actin monomer up to the seventh actin monomer are shown here.

Results. In this instance, we also obtained two models with different orientations. The best-fit model (A-model) is shown in Fig. S4. The root-mean-square errors were 0.123 for the Tn core domain with Ca^{2+} and 0.059 for Tm segment 167–195 with Ca^{2+}. The model in Fig. S4 is approximately equivalent to the model in Fig. 6. This suggests again that small deviations in the probe from the C^{α} positions of the attached amino acid residues do not significantly alter the model.

Figure 7 shows the stereo views for the best-fit model of the Tn core domain, Tm segment 167–195, and F-actin complex without Ca^{2+}. In this model, Tm segment 167–195 is apart from the TnT C-terminal region, and it intrudes into the TnC N-terminal domain, which is unrealistic. When Sun *et al.*[23] attempted to orient the Tn core domain structure without Ca^{2+} on a muscle fiber using polarized fluorescence from bifunctional rhodamine probes on the TnC helices C and E in the muscle fiber, no distribution of orientations of this structure could

reproduce their data. They concluded that the *in situ* conformation of Ca^{2+}-free Tn is significantly different from the crystals of the Ca^{2+}-free core complex. By performing a global search for the rigid-body movements of the crystal structure, we determined the position and orientation of the Tn core domain and Tm on the F-actin filament without altering the crystal structure. For Tm segment 167–195, the root-mean-square errors between the calculated transfer efficiencies and the observed values with Ca^{2+} and without Ca^{2+} were 0.060 and 0.068, respectively. In our previous report, the root-mean-squares for each of the five Tm regions 41–69, 83–111, 146–174, 216–244, and 252–279 were 0.054–0.073. On the other hand, for the Tn core domain, the root-mean-square errors with Ca^{2+} and without Ca^{2+} were 0.119 and 0.132, respectively, which are significantly larger than the values for each Tm region. Because Tm has a simple two-chained α-helical coiled-coil structure, the *in situ* conformation is expected to be similar to

Fig. 7. Stereo views of the best-fit model for the Tn core domain, Tm segment (167–195), and F-actin complex without Ca^{2+}. The Tn subunits C, I, and T are colored green, cyan, and magenta, respectively, and Tm segment 167–195 is colored yellow. The top figure shows the view along the F-actin axis, and the bottom figure shows the view from the pointed end. Only the fifth actin monomer up to the seventh actin monomer are shown here.

the crystal. Therefore, at the best-fit position and orientation, the root-mean-square values were so small. On the other hand, Tn has a multi-subunit structure and a significantly altered conformation in response to Ca^{2+} concentration changes. Tn interacts with Tm in the presence of Ca^{2+} and with both Tm and actin in the absence of Ca^{2+}.[2,24] The structures of the Tn core domain were determined through crystallography without Tm and actin. A large value for the root-mean-square errors at the best-fit position and orientation of the Tn core domain without Ca^{2+} suggests that the conformation of the Tn core domain on the thin filament is significantly different from the crystal structure. Therefore, we must construct a refined atomic model of the thin filament by considering information derived from additional biochemical and biophysical studies. Although there are certain weaknesses in the rigid-body movement method, the angles between the I–T arm and the F-actin axis with and without Ca^{2+} are similar for the data from the fluorescence polarization measurements. Therefore, the general location and orientation of the Tn core domain on the F-actin filament reported herein should be similar to the *in situ* conformation.

Here, we evaluate the atomic models of the actin–Tm complex[19] and the actin–Tm–Tn core domain in relation to the muscle regulation mechanism. The steric blocking model has been widely accepted as the regulation mechanism in which Tm shifts azimuthally around the F-actin axis and physically blocks the myosin-binding site on actin during relaxation. This model has been conceived from the X-ray diffraction studies of muscle fibers in which a significant change in the layer line intensities was observed on whether the muscle was in a relaxed or contracted state.[28–30] These intensity changes were interpreted as an azimuthal shift of the Tm strands on actin. Later kinetic measurements have proposed a three-state model,[31] in which thin filaments exist in rapid equilibrium between three states (blocked or relaxed, closed, and open). Then, the new steric blocking model was proposed, in which Tm shifts azimuthally between three distinct states from 3D-EM.[32]

X-ray intensity changes certainly indicate some conformation changes in the thin filament. However, they cannot be clearly assigned to the azimuthal shift of Tm, since the thin-filament-associated X-ray diffraction intensities as well as

3D-EM have been interpreted based on the assumption that the mass of the Tn/Tm complex is distributed evenly and smoothly all through the continuous Tm strands. It is difficult to deduce the details of the conformational changes in the thin filament only from the X-ray intensity reversal of the fourth-order layer line relative to the second-order layer line. There would be many other explanations for the X-ray intensity changes. On the other hand, in FRET measurements, the energy donor probes were specifically attached to Tm and the energy acceptor probes were attached specifically to F-actin, so that assigning the factor to the change in FRET efficiency is undoubted. FRET showed the absence of a significant azimuthal shift of the Tm strand, in which the positions of five Tm segments on F-actin with or without Ca^{2+} were determined by using 150 FRET efficiencies with or without Ca^{2+} as restraints. The atomic model of the actin–Tm complex also showed that Tm does not uniformly wind around the F-actin filament.[19] Therefore, one should find other explanations for the X-ray intensity changes. The atomic model of the actin–Tn core domain complex shows that the Tn core domain moves toward the actin outer domain and closer to the center of the F-actin axis after Ca^{2+} release from Tn. Squire and Morris suggested that the X-ray intensity changes could be explained as movement of Tn instead of Tm.[33] Our atomic model of the actin–Tm complex on a reconstituted thin filament[19] demonstrated that at a single unique position on the actin molecule, many residues in Tm are involved in electrostatic, hydrogen-bonding, and hydrophobic interactions with actin residues. Although there is no significant Ca^{2+}-induced azimuthal shift, the Ca^{2+}-induced changes in the actin–Tm contact surface are sizable enough to induce a significant conformational change in the F-actin structure, which would be important for muscle regulation. The atomic model of the actin–Tm–Tn core domain showed the orientation and the location of the Tn core domain on the F-actin filament, the interacting residues between the Tn core domain and Tm, and the mass movement of the Tn core domain upon Ca^{2+} binding to Tn. The Ca^{2+}-induced conformational change in the atomic model of the actin–Tm–Tn core domain seems to be consistent with our previously proposed regulation model,[17,34] in which the conformational change of the actin filament induced by the Tn–Tm complex plays an essential role in muscle regulation, instead of Tm blocking the myosin-binding site on actin. On the other hand, the crystal structure of the Tn complex has been revealed only for ∼60% of the mass, and the functionally important regions such as the actin-binding regions are missing. Therefore, we must construct a more refined atomic model of the thin filament in combination with additional biochemical and biophysical methods.

Materials and Methods

Reagents

Amanita phalloides phalloidin was purchased from Sigma. IAEDANS, FLC, and DABMI were purchased from Molecular Probes. TNP-ATP was synthesized according to the method described by Hiratsuka.[35] The microbial transglutaminase was a gift from Ajinomoto Co. All other chemicals were of analytical grade.

Protein preparations

Actin, S1, and Tn were prepared from rabbit skeletal muscle using the procedures from Spudich and Watt,[36] Weeds and Taylor,[37] and Ebashi *et al.*,[38] respectively. Rabbit α-Tm was prepared from rabbit cardiac muscle. Single-cysteine Tm mutants (R167C, S174C, E181C, G188C, and E195C) with an N-terminal extension (AAS) were expressed in *Escherichia coli* and purified as reported by Miki *et al.*[19] To construct single-cysteine TnT25k, TnI, and TnC mutants, we began with the cDNA clones of the rabbit skeletal muscle β-TnT 25-kDa fragment,[39] Cys-less TnI mutant (C48A, C64A, and C133S),[40] and Cys-less TnC (C98I) mutant from Dr. Kayo Maeda. The TnT25k cDNA and TnI cDNA were inserted into the expression vector pTrc99c, and TnC cDNA was inserted into the expression vector pET23d. Using these cDNA-inserted expression vectors, we performed mutagenesis by inverse PCR using the KOD -Plus- Mutagenesis Kit (Toyobo Co., Ltd.) according to the instruction manual. Oligonucleotides used for mutagenesis were synthesized and purified by Invitrogen Life Technologies. All of the mutant expression vectors were confirmed by DNA sequencing (ABI PRISM 310 Genetic analyzer). Protein expression in *E. coli* and purification were carried out according to the method of Fujita-Becker *et al.*[40] The protein concentrations were determined by absorbance using the following extinction coefficients (0.1%): $A_{290\ nm}=0.63$ cm^{-1} (mg/ml)$^{-1}$ for G-actin, $A_{280\ nm}=0.75$ cm^{-1} for S1 and 0.24 cm^{-1} for Tm and the Tm mutants, and $A_{280\ nm}=0.45$ cm^{-1} for Tn. The following relative molecular masses were used: 42 kDa for actin, 115 kDa for S1, 66 kDa for Tm and the Tm mutants, and 69 kDa for Tn.

Protein labeling

Actin Cys374 and Gln41 were labeled with DABMI and FLC, respectively, and F-actin-bound ADP was replaced with TNP-ADP as we reported previously.[19] All of the single-cysteine Tm mutants were labeled with IAEDANS as we reported previously.[19] All of the single-cysteine TnT25k, TnI, and TnC mutants were labeled with IAEDANS as we reported previously.[18] Reconstruction of the AEDANS–Tn complex was performed according to the method of Fujita-Becker *et al.*[40] The AEDANS-labeled single-cysteine mutants for TnT25k, TnI, or TnC with additional unlabeled Tn subunit components were

dissolved in 6 M urea, 50 mM Tris–HCl (pH 8.0), 1 mM DTT, 1 mM NaN_3, and 0.1 mM PMSF. Each Tn subunit was mixed at the molar ratio 1:1:1 and incubated at 4 °C for 30 min. The mixture was dialyzed against 0.1 M K-phosphate buffer (pH 7.5) with 1 mM DTT and 1 mM NaN_3 and applied to a Q-Sepharose fast flow column (2.5 cm×10 cm) equilibrated with 0.1 M K-phosphate buffer (pH 7.5) and 1 mM DTT. The reconstituted Tn complex was eluted from the column with 0.2 M KCl. Fractions containing the reconstituted Tn complex were pooled, and the protein was precipitated with 66% saturated ammonium sulfate at 10,000 g for 20 min. The pellet was dissolved in 10 mM Tris–HCl (pH 8.0), 0.1 M KCl, 1 mM DTT, 1 mM NaN_3, and 0.1 mM PMSF and then dialyzed against the same buffer solution.

ATPase measurements

The biochemical activities of the AEDANS–Tm and AEDANS–Tn complex were assayed through Ca^{2+}-dependent regulation of the acto-S1 ATPase activity. The measurements were performed at 25 °C in 10 mM KCl, 5 mM $MgCl_2$, 2 mM ATP, 20 mM Tris–HCl (pH 7.6), 1 mM DTT, and either 50 μM $CaCl_2$ for the $+Ca^{2+}$ state or 1 mM ethylene glycol bis(β-aminoethyl ether)N,N'-tetraacetic acid (EGTA) for the $-Ca^{2+}$ state. The protein concentrations used were 4 μM F-actin, 0.57 μM Tm, 0.67 μM Tn, and 1 μM S1. The amount of inorganic phosphate released was determined colorimetrically, according to the method of Tausky and Shorr.[41]

Fluorescence measurements

The steady-state fluorescence was measured using a Hitachi F-4500 fluorometer. The time-resolved fluorescence lifetime measurements were performed with a Horiba (IBH) 5000U fluorometer equipped with a 337-nm LED light source as we reported previously.[19]

Fluorescence resonance energy transfer

The efficiency (E) of the resonance energy transfer between probes was determined by measuring either the donor fluorescence intensity or the fluorescence lifetime, with the acceptor (F_{DA}, $\langle\tau\rangle_{DA}$) and without the acceptor (F_{D0}, $\langle\tau\rangle_{D0}$) as described by Lakowicz:[21]

$$E = 1 - F_{DA}/F_{D0} = 1 - \langle\tau\rangle_{DA} / \langle\tau\rangle_{D0} \qquad (2)$$

where $\langle\tau\rangle$ ($= \Sigma \ \alpha_i\tau_i$) is the lifetime-weighted quantum yield, which is proportional to the area under the decay curve for the lifetime ($\int_0^\infty I(t)dt$). Details are described in Supplementary Information.

For a single donor and either a single or multiple acceptors, the transfer efficiency is related to the ith donor–acceptor distance (r_i) and Förster's critical distance (R_0), at which the transfer efficiency is equal to 50%:

$$\sum_i R_0^6/r_i^6 = \left(E^{-1}-1\right)^{-1} \qquad (3)$$

Förster's critical distance, R_0, can be obtained (in nanometers) using the following equation:

$$R_0^6 = \left(8.79 \times 10^{-11}\right)n^{-4} \ \kappa^2 \ Q_0 J \qquad (4)$$

n is the medium refractive index (1.4), κ^2 is the orientation factor, Q_0 is the donor quantum yield without the acceptor, and J is the spectral overlap integral between the donor emission $F_D (\lambda)$ and the acceptor absorption $\varepsilon_A(\lambda)$ spectra, which is defined in the following equation:

$$J = \int F_D(\lambda)\varepsilon_A(\lambda)\lambda^4 \, d\lambda / \int F_D(\lambda) \, d\lambda \qquad (5)$$

The quantum yield (Q_0) for AEDANS attached to TnI-133 on the reconstituted thin filament with Ca^{2+} was 0.27,[18] and the lifetime-weighted quantum yield ($\langle\tau\rangle$) was 13.82 ns. As the lifetime-weighted quantum yields are proportional to the quantum yields, the quantum yields for AEDANS attached to the single-cysteine Tn mutants on the reconstituted thin filaments were determined by measuring the lifetime-weighted quantum yields with and without Ca^{2+}. The overlap integrals (J) were calculated as 6.74×10^{14}, 7.54×10^{14}, and 18.7×10^{14} (M^{-1} cm^{-1} nm^4) for the AEDANS-Tm/DAB-F-actin, AEDANS-Tm/TNP-ADP-F-actin, and AEDANS-Tm/FLC-F-actin pairs, respectively. $\kappa^2 = 2/3$ for the calculation of R_0.

Simulation of FRET efficiency

Energy is transferred from an excited donor (AEDANS) on the Tn complex to acceptors on the five neighboring actin monomers. The transfer efficiency can be calculated according to our previous report.[19] With two possibilities for an acceptor on each actin monomer (present or absent), an excited donor has $2^5 = 32$ possible configurations. Here, the labeling ratio of acceptor (A/P) is denoted as p. The normalized fluorescence intensity [$F(p)$] of the donor on the Tn complex in the presence of acceptors on F-actin (acceptor labeling ratio p) was calculated using the following equation:

$$F(p) = \sum_{i=1}^{32}(f_i / f_0)\alpha_i \qquad (6)$$

where α_i is the probability of the ith configuration obtained by calculating the polynomial distribution.[19] f_0 and f_i are the fluorescence intensities with and without the acceptor, respectively:

$$f_i = f_0 / \left\{1 + \sum_{m=1}^{n} (R_0 / r_m)^6\right\} \qquad (7)$$

where n is the number of acceptors in the five adjacent actin monomers that are in the ith configuration; r_m is the distance between the donor and the acceptor, which can be calculated at each orientation of the Tn core domain on F-actin in rigid body translation and rotation; and R_0 is Förster's critical distance.

The transfer efficiency $E_{calc}(p)$ at the labeling ratio p was calculated using the following equation:

$$E_{calc}(p) = 1 - F(p) \qquad (8)$$

Because Tm consists of two chains, the fluorescence intensity $F_{av}(p)$ of the donors on a single-cysteine Tm mutant is the average of the two donors on both chains: $(F_1(p) + F_2(p))/2$. Thus, the transfer efficiency $E_{calc}(p)$ at the labeling ratio p was calculated using the following equation:

$$E_{calc}(p) = 1 - F_{av}(p) \qquad (9)$$

Acknowledgements

Supplementary Data

Supplementary data associated with this article can be found, in the online version, at doi:10.1016/ j.jmb.2012.03.029

References

1. Ebashi, S., Endo, M. & Ohtsuki, I. (1969). Control of muscle contraction. *Q. Rev. Biophys.* **2**, 351–384.
2. Perry, S. V. (2001). Vertebrate tropomyosin: distribution, properties and function. *J. Muscle Res. Cell Motil.* **22**, 5–49.
3. Kabsch, W., Mannherz, H. G., Suck, D., Pai, E. F. & Holmes, K. C. (1990). Atomic structure of the actin: DNase I complex. *Nature*, **347**, 37–44.
4. Whitby, F. G. & Phillips, G. N. (2000). Crystal structure of tropomyosin at 7 Angstroms resolution. *Proteins: Struct. Funct. Genet.* **38**, 49–59.
5. Takeda, S., Yamashita, A., Maeda, K. & Maéda, Y. (2003). Structure of the core domain of human cardiac troponin in the Ca^{2+}-saturated form. *Nature*, **424**, 35–41.
6. Vinogradova, M. V., Stone, D. B., Malanina, G. G., Karatzaferi, C., Cooke, R., Mendelson, R. A. & Fletterick, R. J. (2005). Ca^{2+}-regulated structural changes in troponin. *Proc. Natl Acad. Sci. USA*, **102**, 5038–5043.
7. Holmes, K. C., Popp, D., Gebhard, W. & Kabsch, W. (1990). Atomic model of the actin filament. *Nature*, **347**, 44–49.
8. Lorenz, M., Popp, D. & Holmes, K. C. (1993). Refinement of the F-actin model against x-ray fiber diffraction data by the use of a directed mutation algorithm. *J. Mol. Biol.* **234**, 826–836.
9. Oda, T., Iwasa, M., Aihara, T., Maéda, Y. & Narita, A. (2009). The nature of the globular- to fibrous-actin transition. *Nature*, **457**, 441–445.
10. Fujii, T., Iwane, A. H., Yanagida, T. & Namba, K. (2010). Direct visualization of secondary structures of F-actin by electron cryomicroscopy. *Nature*, **467**, 724–728.
11. Narita, A., Yasunaga, T., Ishikawa, T., Mayanagi, K. & Wakabayashi, T. (2001). Ca^{2+}-induced switching of troponin and tropomyosin on actin filaments as revealed by electron cryo-microscopy. *J. Mol. Biol.* **308**, 241–261.
12. Murakami, K., Yumoto, F., Ohki, S., Yasunaga, T., Tanokura, M. & Wakabayashi, T. (2005). Structural basis for Ca^{2+}-regulated muscle relaxation at interaction sites of troponin with actin and tropomyosin. *J. Mol. Biol.* **352**, 178–201.
13. Pirani, A., Vinogradova, M., Curmi, P., King, W., Fletterick, R., Craig, R. *et al.* (2006). An atomic model of the thin filament in the relaxed and Ca^{2+}-activated states. *J. Mol. Biol.* **357**, 1–11.
14. Paul, D., Morris, E., Kensler, R. & Squire, J. (2009). Structure and orientation of troponin in the thin filament. *J. Biol. Chem.* **284**, 15007–15015.
15. Poole, K. J. V., Lorenz, M., Evans, G., Rosenbaum, G., Pirani, A., Craig, R. *et al.* (2006). A comparison of muscle thin filament models obtained from electron microscopy reconstructions and low-angle X-ray fibre diagrams from non-overlap muscle. *J. Struct. Biol.* **155**, 273–284.
16. dos Remedios, C. G. & Moens, P. D. J. (1995). Fluorescence resonance energy transfer spectroscopy is a reliable "Ruler" for measuring structural changes in proteins: dispelling the problem of the unknown orientation factor. *J. Struct. Biol.* **115**, 175–185.
17. Miki, M. (2007). Conformational changes in reconstituted skeletal muscle thin filaments observed by fluorescence spectroscopy. *Adv. Exp. Med. Biol.* **592**, 111–123.
18. Kimura-Sakiyama, C., Ueno, Y., Wakabayashi, K. & Miki, M. (2008). Fluorescence resonance energy transfer between residues on troponin and tropomyosin in the reconstituted thin filament: modeling the troponin–tropomyosin complex. *J. Mol. Biol.* **376**, 80–91.
19. Miki, M., Makimura, S., Saitoh, T., Bunya, M., Sugahara, Y., Ueno, Y. *et al.* (2011). A three-dimensional FRET analysis to construct an atomic model of the actin–tropomyosin complex on a reconstituted thin filament. *J. Mol. Biol.* **414**, 765–782.
20. Miki, M., Hai, H., Saeki, K., Shitaka, Y., Sano, K. I., Maéda, Y. & Wakabayashi, T. (2004). Fluorescence resonance energy transfer between points on actin and the C-terminal region of tropomyosin in skeletal muscle thin filaments. *J. Biochem. (Tokyo)*, **136**, 39–47.
21. Lakowicz, J. R. (1999). *Principles of Fluorescence Spectroscopy*, 2nd edit. Kluwer Academic/Plenum Publishers, New York, NY.
22. Flaherty, K. M., McKay, D. B., Kabsch, W. & Holmes, K. C. (1991). Similarity of the three-dimensional structures of actin and the ATPase fragment of a 70-kDa heat shock cognate protein. *Proc. Natl Acad. Sci. USA*, **88**, 5041–5045.
23. Sun, Y. B., Brandmeier, B. & Irving, M. (2006). Structural changes in troponin in response to Ca^{2+} and myosin binding to thin filaments during activation of skeletal muscle. *Proc. Natl Acad. Sci. USA*, **103**, 17771–17776.

24. Ohtsuki, I. (2007). Troponin: structure, function and dysfunction. *Adv. Exp. Med. Biol.* **592**, 21–36.
25. Brown, J. H., Kim, K. H., Jun, G., Greenfield, N. J., Dominguez, R., Volkmann, N. *et al.* (2001). Deciphering the design of the tropomyosin molecule. *Proc. Natl Acad. Sci. USA*, **98**, 8496–8501.
26. Brown, J. H., Zhou, Z., Reshetnikova, L., Robinson, H., Yammani, R. D., Tobacman, L. S. & Cohen, C. (2005). Structure of the mid-region of tropomyosin: bending and binding sites for actin. *Proc. Natl Acad. Sci. USA*, **102**, 18878–18883.
27. Hitchcock-DeGregori, S. E. & Singh, A. (2011). What makes tropomyosin an actin binding protein? A perspective. *J. Struct. Biol.* **170**, 319–324.
28. Haselgrove, J. C. (1972). X-ray evidence for a conformational change in the actin-containing filaments of vertebrate striated muscle. *Cold Spring Harbor Symp. Quant. Biol.* **37**, 341–352.
29. Huxley, H. E. (1972). Structural changes in the actin and myosin-containing filaments during contraction. *Cold Spring Harbor Symp. Quant. Biol.* **37**, 361–376.
30. Parry, D. A. & Squire, J. M. (1973). Structural role of tropomyosin in muscle regulation: analysis of the x-ray diffraction patterns from relaxed and contracting muscles. *J. Mol. Biol.* **75**, 33–55.
31. McKillop, D. F. & Geeves, M. A. (1993). Regulation of the interaction between actin and myosin subfragment 1: evidence for three states of the thin filament. *Biophys. J.* **65**, 693–701.
32. Vibert, P., Craig, R. & Lehman, W. (1997). Steric-model for activation of muscle thin filaments. *J. Mol. Biol.* **266**, 8–14.
33. Squire, J. M. & Morris, E. P. (1998). A new look at thin filament regulation in vertebrate skeletal muscle. *FASEB J.* **12**, 761–771.

34. Kimura, C., Maeda, K., Maéda, Y. & Miki, M. (2002). Ca^{2+}- and S1-induced movement of troponin T on reconstituted skeletal muscle thin filaments observed by fluorescence energy transfer spectroscopy. *J. Biochem. (Tokyo)*, **132**, 93–102.
35. Hiratsuka, T. (1982). Biological activities and spectroscopic properties of chromophoric and fluorescent analogs of adenine nucleoside and nucleotides, 2′, 3′-*O*-(2,4,6-trinitrocyclohexadienylidene) adenosine derivatives. *Biochim. Biophys. Acta*, **719**, 509–517.
36. Spudich, J. A. & Watt, S. (1971). The regulation of rabbit skeletal muscle contraction. I. Biochemical studies of the interaction of the tropomyosin–troponin complex with actin and the proteolytic fragments of myosin. *J. Biol. Chem.* **246**, 4866–4871.
37. Weeds, A. G. & Taylor, R. S. (1975). Studies on the chymotryptic digestion of myosin. Effects of divalent cations on proteolytic susceptibility. *Nature*, **257**, 54–56.
38. Ebashi, S., Wakabayashi, T. & Ebashi, F. (1971). Troponin and its components. *J. Biochem. (Tokyo)*, **69**, 441–445.
39. Fujita, S., Maeda, K. & Maéda, Y. (1991). Complete coding sequences of cDNAs of four variants of rabbit skeletal muscle troponin T. *J. Muscle Res. Cell Motil.* **12**, 560–565.
40. Fujita-Becker, S., Kluwe, L., Miegel, A., Maeda, K. & Maéda, Y. (1993). Reconstitution of rabbit skeletal muscle troponin from the recombinant subunits all expressed in and purified from *E. coli*. *J. Biochem. (Tokyo)*, **114**, 438–444.
41. Tausky, H. H. & Shorr, E. (1953). A microcolorimetric method for the determination of inorganic phosphorus. *J. Biol. Chem.* **202**, 675–685.

Time-resolved fluorescence lifetime measurements. In the multi-exponential model the intensity is assumed to decay as the sum of individual single-exponential decays:

$$I(t) = \sum_{i=1}^{n} \alpha_i \exp(-t/\tau_i) \qquad \text{(eq. 1)}$$

The lifetime-weighted quantum yield was given by

$$\langle\tau\rangle = \sum_{i=1}^{n} \alpha_i\tau_i \qquad \text{(eq. 2)}$$

For a double-exponential decay it becomes

$$\int_{0}^{\infty} I(t)\mathrm{d}t = \alpha_1\tau_1 + \alpha_2\tau_2 \qquad \text{(eq. 3)}$$

$\langle\tau\rangle$ is proportional to the area under the decay curve of the lifetime, so that it is called as a lifetime-weighted quantum yield. The transfer efficiencies were determined by the lifetime-weighted quantum yield ($\langle\tau\rangle = \sum \alpha_i\tau_i$) with ($\langle\tau\rangle_{DA}$) and without ($\langle\tau\rangle_{D0}$) the acceptor.

$$E = 1 - \langle\tau\rangle_{DA}/\langle\tau\rangle_{D0} \qquad \text{(eq. 4)}$$
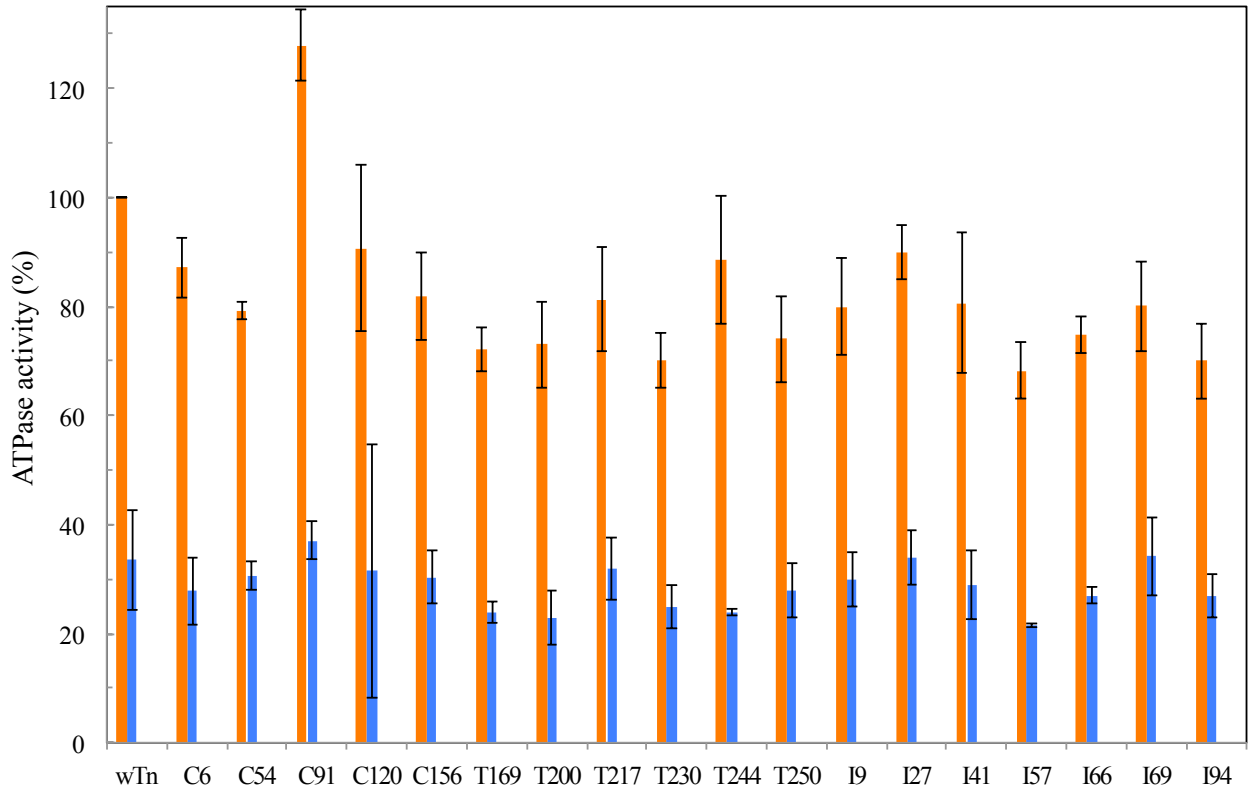
Fig. S1. Ca^{2+}-dependent regulation of acto-S1-ATPase by the labeled Tn mutants. The reactions were carried out at 25 $^{\circ}$C with 4 µM F-actin, 1 µM rabbit skeletal S1, 0.57 µM Tm, and 0.67 µM Tn in 10 mM KCl, 5 mM $MgCl_2$, 1 mM DTT, 2 mM ATP, and 20 mM MOPS (pH 7.0) in the presence of 50 µM $CaCl_2$ (orange bar graphs) or 1 mM EGTA (blue bar graphs). The value of 100 represents the ATPase activity of actoS1 with rabbit skeletal muscle Tn and αTm with Ca^{2+} under the same experimental conditions.
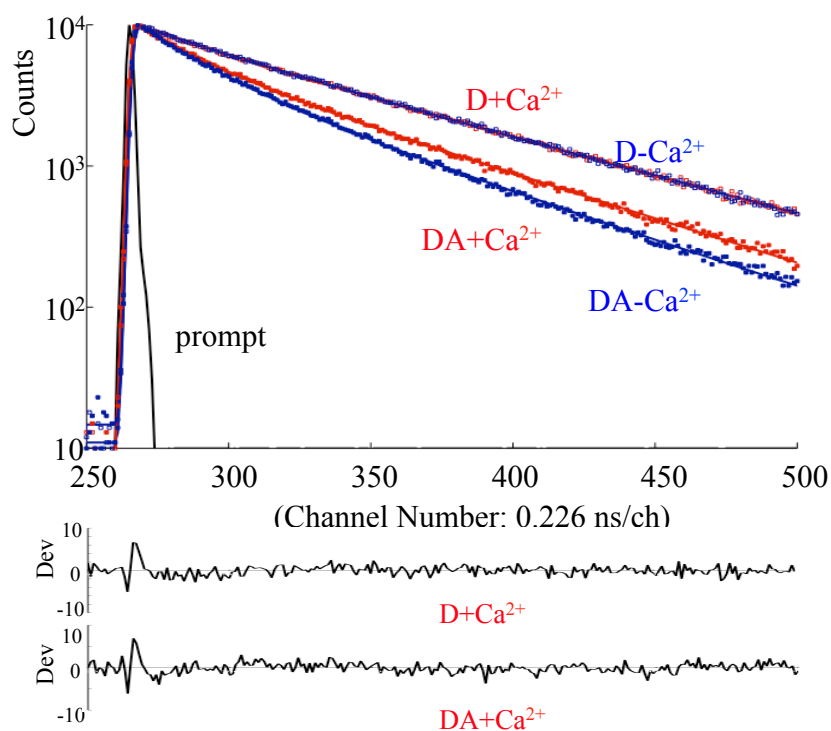
Fig. S2. Fluorescence intensity decay curves for the donor-AEDANS attached to the Tn core domain (TnT230) in the reconstituted thin filament with and without acceptor-DABMI in the presence (red) and absence (blue) of Ca^{2+}. The sharp peak on the left is due to the excitation light pulse. The decays were measured with excitation at 337 nm, and the emission was collected at 490 nm. A sharp cut-off filter SC-42 (Fuji Film) was placed on the emission side. Blank- and filled-square plots show the fluorescence intensity decay curves of the donor in the absence and presence of acceptor-DABM attached to Cys374 of actin, respectively. The smooth lines show the decay curves calculated with two exponential lifetimes. The residual plots of the fit are displayed in the lower space across the figure. Samples were in a buffer of 30 mM KCl, 2 mM $MgCl_2$, 20 mM Tris–HCl (pH 7.6), 1 mM NaN_3, and either 50 μM $CaCl_2$ for the +Ca^{2+} state or 1 mM EGTA for the –Ca^{2+} state.
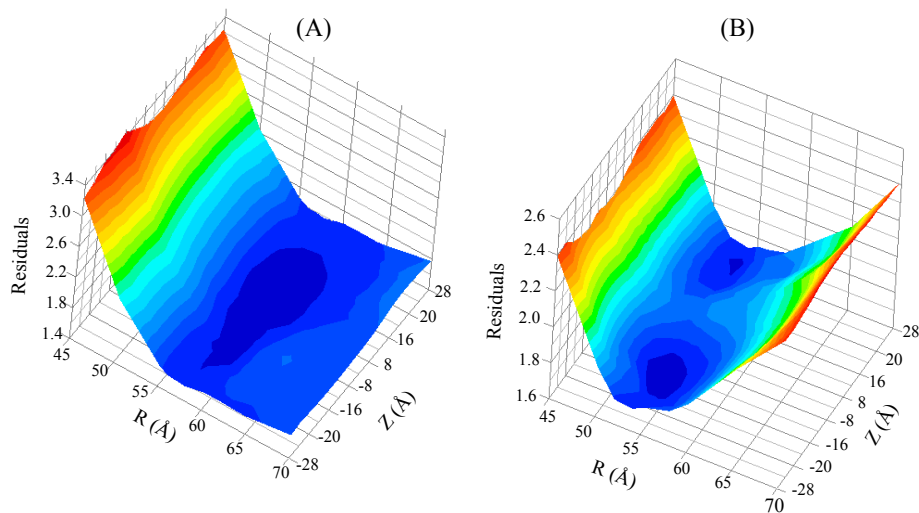
Fig. S3. A three-dimensional map of the residuals as a function of R and Z in the presence (A) and absence (B) of Ca^{2+}.
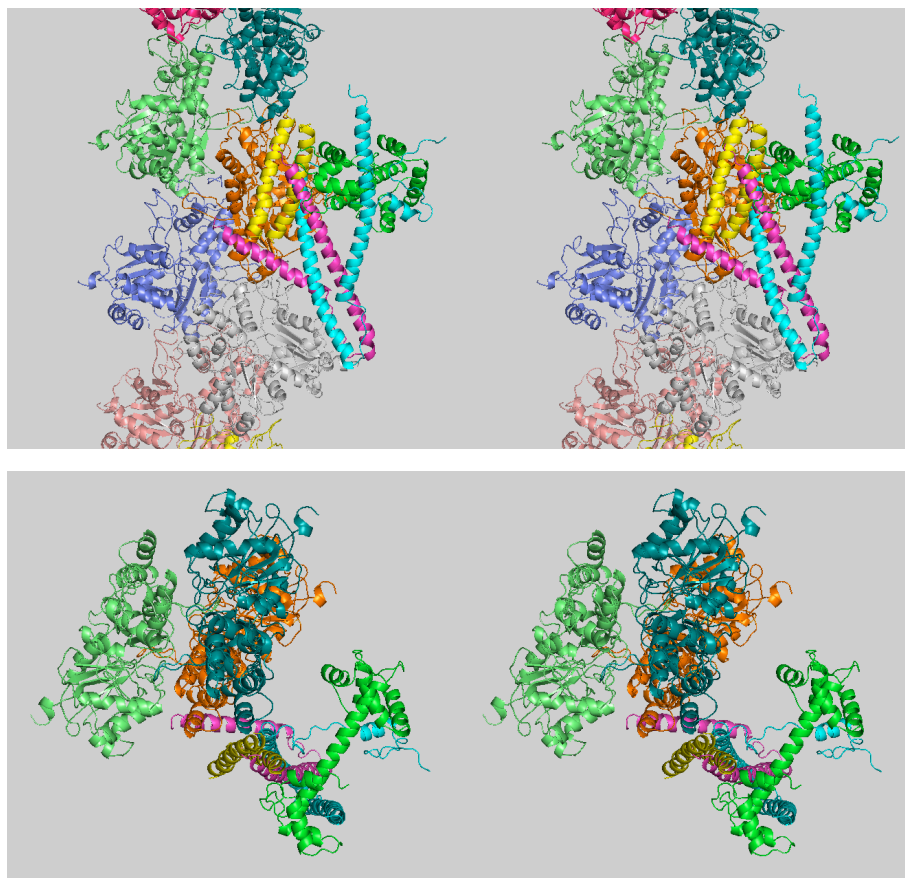
Fig. S4. Stereo views of the best-fit model for the Tn core domain, Tm segment (167–195), and F-actin complex in the presence of Ca^{2+}. The atomic coordinates from Lorenz *et al.*'s F-actin model, instead of Fujii *et al.*'s F-actin model, were used for calculation to construct the model.